



OPEN Abnormal ac4C modification in metabolic dysfunction associated steatotic liver cells

Xiqian Zhang¹, Yaxian Zheng¹, Jing Yang¹, Yan Yang¹, Qin He¹, Min Xu¹, Fangyi Long²✉ & Yujie Yang¹✉

The pathogenesis of metabolic dysfunction-associated steatotic liver disease (MASLD) remains unclear due to the complexity of its etiology. The emerging field of the epitranscriptome has shown significant promise in advancing the understanding of disease pathogenesis and developing new therapeutic approaches. Recent research has demonstrated that N4-acetylcytosine (ac4C), an RNA modification within the epitranscriptome, is implicated in progression of various diseases. However, the role of ac4C modification in MASLD remains unexplored. Herein, we performed acRIP-ac4c-seq and RNA-seq analysis in free fatty acids-induced MASLD model cells, identifying 2128 differentially acetylated ac4C sites, with 1031 hyperacetylated and 1097 hypoacetylated peaks in MASLD model cells. Functional enrichments analysis showed that ac4C differentially modified genes were significantly involved in processes related to MASLD, such as nuclear transport and MAP kinase (MAPK) signaling pathway. We also identified 341 differentially expressed genes (DEGs), including 61 lncRNAs and 280 mRNAs, between control and MASLD model cells. Bioinformatics analysis showed that DEGs were significantly enriched in long-chain fatty acid biosynthetic process. Notably, 118 genes exhibited significant changes in both ac4C modification and expression levels in MASLD model cells. Among these proteins, JUN, caveolin-1 (CAV1), fatty acid synthase (FASN), and heterogeneous nuclear ribonucleoprotein A1 (hnRNPA1) were identified as core proteins through protein–protein interaction (PPI) network analysis using cytoscape software. Collectively, our findings establish a positive correlation between ac4C modification and the pathogenesis of MASLD and suggest that ac4C modification may serve as a therapeutic target for MASLD.

Keywords MASLD, Epitranscriptome, ac4C

Abbreviations

MASLD	Metabolic dysfunction-associated steatotic liver disease
ac4C	N4-acetylcytosine
NAT10	N-acetyltransferase 10
FFAs	Free fatty acids
DEGs	Differentially expressed genes
ADMGs	Ac4C differentially modified genes
PPI	Protein–protein interaction
CAV1	Caveolin-1
FASN	Fatty acid synthase
hnRNPA1	Heterogeneous nuclear ribonucleoprotein A1
MASH	Metabolic dysfunction-associated steatohepatitis
MDA	Malondialdehyde
TG	Triglyceride
ROS	Reactive oxygen species

Metabolic dysfunction-associated steatotic liver disease (MASLD), previously known as non-alcoholic fatty liver disease (NAFLD), is regarded as the liver manifestation of metabolic syndrome. MASLD affects approximately

¹Department of Pharmacy, Affiliated Hospital of Southwest Jiao Tong University, The Third People's Hospital of Chengdu, Chengdu 610014, China. ²Laboratory Medicine Center, Sichuan Provincial Women's and Children's Hospital, Affiliated Women's and Children's Hospital of Chengdu Medical College, Chengdu Medical College, Chengdu 610041, China. ✉email: longfangyi@cmc.edu.cn; yangyujie@swjtu.edu.cn

1.7 billion individuals worldwide, with a global prevalence approximately 25%. In developed regions, the prevalence rate surpasses 30% and reaches 27% in Asia, with 10–30% of MASLD cases advancing to metabolic dysfunction-associated steatohepatitis (MASH), previously known as non-alcoholic steatohepatitis (NASH)^{1–4}. The rising incidence of obesity worldwide has contributed to an increase in MASLD cases, affecting increasingly younger populations. Despite its prevalence, few effective clinical treatments for MASLD are available due to the uncertain pathogenesis. Consequently, it is crucial to deepen our understanding of MASLD's underlying mechanisms to identify novel preventive and therapeutic strategies.

With the in-depth exploration in the field of epigenetics, numerous emerging epigenetic regulatory mechanisms have been discovered. Epitranscriptome modification, also known as RNA modification, is an important component of epigenetic regulation. Over 170 chemical modifications have been identified in RNA, primarily in non-coding RNAs⁵. Advances in genomic microarray technology and genome and transcriptome sequencing have enabled the identification of diverse RNA modifications, including N6-methyladenine (m6A), N1-methyladenine (m1A), 5-methylcytosine (m5C), 5-hydroxymethylcytosine (hm5C), N7-methylguanine (m7G), and N4-acetylcytosine (ac4C), which impact mRNA expression, metabolism, and function^{5,6}. These modifications are usually regulated by a series of functional proteins, including one or more of modification enzymes (writers), demodification enzymes (erasers) and modification recognition proteins (readers)⁷. With the continuous discovery of new functional proteins, the reversible changes in dynamic regulation of mRNA modifications have received extensive attention and investigation in the prevention and treatment of human diseases.

ac4C, the first acetylation identified in mRNAs, is abundantly present in the human transcriptome, predominantly in coding sequence (CDS) regions. Given its extensive acetylation targets in the human genome, ac4C has emerged as a critical component of the epitranscriptome^{8,9}. Current research indicates that ac4C modification is regulated exclusively by the enzyme N-acetyltransferase 10 (NAT10), the only known enzyme with both acetylation catalytic activity and RNA-binding capacity¹⁰. Altered ac4C levels have been observed in some diseases, such as systemic lupus erythematosus (SLE) and human immunodeficiency virus 1 (HIV-1) infection^{11,12}. However, the role of ac4C modification in MASLD remains largely unstudied.

In this study, we employed transcriptome sequencing (RNA-seq) and acetylated RNA immunoprecipitation sequencing (acRIP-seq) to characterize ac4C mRNA modifications in MASLD cells. The results demonstrated notable ac4C modifications in MASLD cells. Gene ontology (GO) and Kyoto Encyclopedia of Genes and Genomes (KEGG) analysis indicated that the modified and differentially expressed mRNAs were significantly enriched in the lipid synthesis and metabolism pathways. These findings highlight the involvement of ac4C RNA acetylation in MASLD development, offering novel insights into MASLD pathogenesis and potential prevention strategies.

Materials and methods

Cell experiments and sample collection

The hepatic stem cell line HepaRG was purchased from Shanghai Honsun Biological Technology Co., Ltd (Shanghai, China). The cells, at a density of 2.5×10^4 cells/cm, were cultured in Roswell Park Memorial Institute 1640 medium (HyClone, USA) supplemented with 100 units/mL penicillin, 100 µg/mL streptomycin, 5 µg/ml insulin, 50 µM hydrocortisone hemisuccinate, and 10% FBS at 37 °C in a humidified atmosphere with 5% CO₂. Cells were differentiated by incubating in 1.7% dimethyl sulfoxide (DMSO) for 2 weeks. The cultivation of MASLD model cells were conducted as previously described¹³. In brief, the differentiated cells were treated with serum-free medium containing free fatty acids (FFAs), 0.25 mmol/L palmitic acid (PA), 0.5 mmol/L oleic acid (OA), for 24 h. Then, the cells were harvested with TRNzol (TIANGEN, China) for further analysis.

Oil red O staining

Lipid accumulation in MASLD model cells was evaluated via oil red O staining using Modified Lipid Staining Kit (Beyotime, China) according to the manufacturer's protocols. Briefly, cells were rinsed with PBS for 3 times, and then fixed with 4% paraformaldehyde for 10 min. The cells were then covered with staining wash solution for 20 s, followed by immersion in oil red O staining solution for 20 min. The staining solution was removed by washing, and the samples were rinsed with PBS. The stained cells were observed by microscope and photographed.

Biochemical analysis

The malondialdehyde (MDA), triglyceride (TG), and total cholesterol levels in cells were determined using commercial test kits (Jiancheng, China). Cell samples were processed following the manufacturer's instructions. Optical density (OD) values were determined by a VICTOR Nivo Multimode Microplate Reader (Revvity, USA) and the contents of biochemical indicators in cells were calculated according to the kits' protocols. The content of reactive oxygen species (ROS) was analyzed by flow cytometer CytoFLEX (Beckman coulter, USA). The data for 10,000 cells were collected and evaluated using FlowJo V10.4 software (Tree Star, Inc., USA).

acRIP-ac4c-seq and RNA-seq analysis

The acRIP-ac4c-seq and RNA-seq services were provided by Genechem Co., Ltd. (Shanghai, China). The overall experimental process and analytical workflow are shown in Fig. 1A–B. Briefly, Qubit RNA HS kit (Invitrogen, USA) was used to determine the concentration of total RNA extracted with TRNzol Reagent. RNA was digested with the fragmentation buffer into fragments of approximately 100–200 nt. Acetylated RNA enrichment was performed using EpiTM ac4C immunoprecipitation kit according to the commercial protocol (EpiBiotek, R1815). The digested RNA samples were then incubated with an anti-ac4C antibody (Abcam, ab252215) for 3 h at 4 °C. Antibody-protein-RNA complexes were enriched by incubation with protein A/G beads for 2 h at 4 °C and then eluted using RNA clean kit (Zymo Research, R1017) to gain the ac4C-enriched RNA. RNA libraries

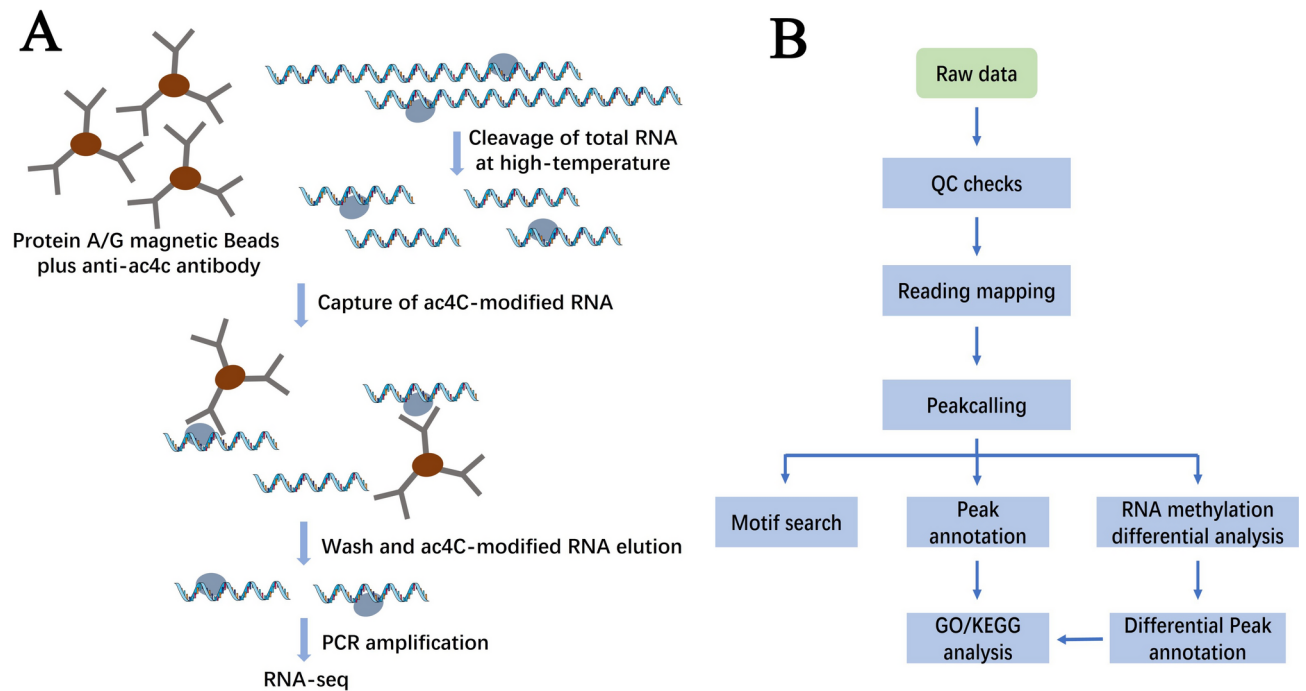


Fig. 1. Schematic of the acRIP-ac4c-seq procedure. (A) Experimental process. (B) Analytical workflow.

Oligo name	Sequence (5'→3')
Human-JUN-forward	AACAGAGCATGACCCTGAAC
Human-JUN-reverse	CCGTTGCTGGACTGGATTAT
Human-CAV1-forward	CAACATCTACAAGCCCAACAAC
Human-CAV1-reverse	TCCCTTCTGGTTCTGCAATC
Human-FASN-forward	CTGAAGGACCTGTCTAGGTTTG
Human-FASN-reverse	CGGAGTGAATCTGGGTTGAT
Human-hnRNPA1-forward	GGATGGCTATAATGGATTTGGTAATG
Human-hnRNPA1-reverse	AAATTTCCCTCCCTTCATGGGT
Human-GAPDH-forward	GTCAACGGATTTGGTCGATTG
Human-GAPDH-reverse	TGTAGTTGAGGTCAATGAAGGG

Table 1. Oligonucleotide primers for gene expression.

for input and the ac4C IP samples were constructed by EpiTM mini long RNA-seq kit (Epibiotek, E1802). All samples were subjected to 150-bp paired-end sequencing on an Illumina NovaSeq 6000 sequencer. After adapter-trimming and sequence-filtering using cutadapt (v2.5), clean reads were then aligned to the human Ensemble genome GRCh38 by Hisat2 (v2.1.0). Acetylated sites and differential ac4C peaks were identified by exomePeak R package (v2.13.2). The input samples were used for RNA-seq analysis, and featureCounts (v1.6.3) was used to map reads to the genome. The DESeq2 R-package and clusterprofile R package (v3.6.0) were used for differential gene expression analysis and GO/KEGG analysis.

Protein–protein interaction (PPI) network analysis

The information of a total of 118 genes which both significantly changed in ac4C modification and expression levels in MASLD model cells (P value < 0.05) was imported into the string website (<https://cn.string-db.org/>) for gene interaction analysis, and the results were then imported into cytoscape software (v3.9.1) to obtain the PPI network diagram.

Quantitative real-time polymerase chain reaction

Total RNA was extracted from the HepaRG cells using TRNzol (TIANGEN, China) following commercial instructions. The preparation of complementary DNA (cDNA) was performed by a reverse transcription kit (Vazyme, China). mRNA amplification was conducted by the SYBR qPCR Master Mix (Vazyme, China). The primer sequences are listed in Table 1. Gene expression was normalized to that of GAPDH. The fold changes of mRNA quantification of the genes were calculated using the $2^{-\Delta\Delta CT}$ method.

Western blotting

Protein was extracted from the HepaRG cells using Radio-Immunoprecipitation Assay (RIPA) buffer (Wanlei, China). The protein concentration was determined by the bicinchoninic acid (BCA) kit (Wanlei, China). The protein was separated on dodecylsulphate polyacrylamide gel electrophoresis and transferred onto the polyvinylidene fluoride membrane (Millipore, USA). After incubation with the primary antibodies (anti-JUN (Proteintech, 24,909-1-AP), anti-CAVI (Proteintech, 16,447-1-AP), anti-FASN (Proteintech, 10,624-2-AP), anti-hnRNPA1 (Proteintech, 11,176-1-AP), and anti-GAPDH antibodies (Proteintech, 60,004-1-Ig)) overnight at 4 °C, the membranes were further incubated with secondary antibodies for 1 h at room temperature. The quantification of immunoblotting was achieved by Image J software.

Statistical analysis

Experimental data were displayed as mean \pm SD and were statistically analyzed in GraphPad Prism 8 software (GraphPad, USA) with the two-tailed Student's t-test. The P value < 0.05 was defined to be statistically significant.

Results

MASLD model cells construction

The successful establishment of the MASLD model cells was verified through optical microscopy, oil red O staining, and biochemical indicators analysis. Cells in control group exhibited normal morphology (Fig. 2A), whereas those in the model group cells showed significant lipid droplet accumulation. Furthermore, oil red O staining revealed extensive red lipid droplets in the cytoplasm of the model group, indicating high lipid content and large droplet size (Fig. 2B). Compared with those in normal group, the levels of MDA, TG, total cholesterol, and ROS in cells were significantly increased in model group (Fig. 2C–F).

Whole-transcriptome profiling of ac4C modifications in control and MASLD model cells

Using the exomePeak R package for peak calling and analysis, we identified 60,651 and 61,434 ac4C peaks on transcriptome in control and MASLD model cells, respectively, including mRNA, lncRNA, miscellaneous

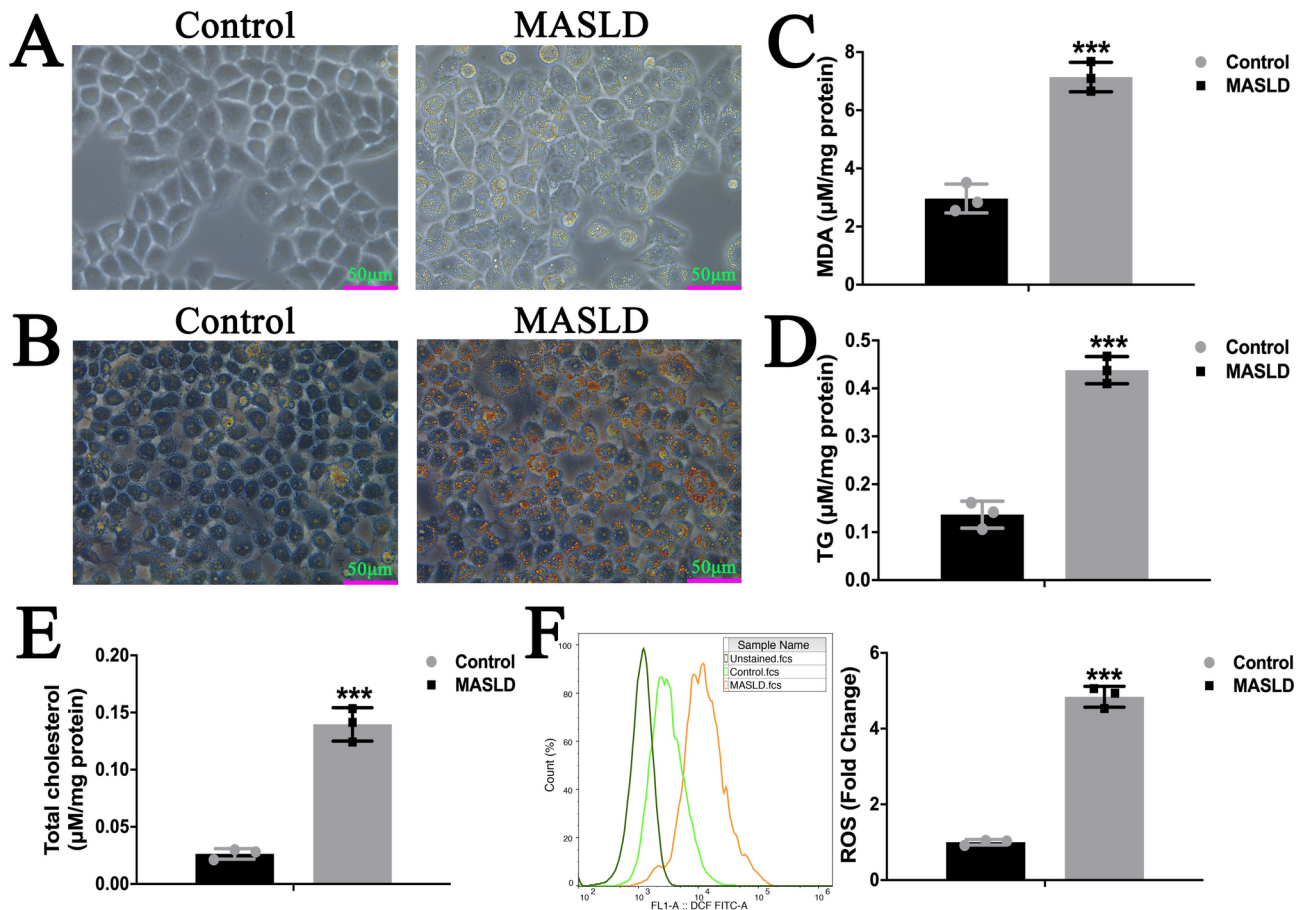


Fig. 2. FFA induced steatosis in control and MASLD model cells. Representative bright field microscopy images of control and MASLD model cells in native (A) and Oil red O stained conditions (B). The levels of MDA (C), TG (D), total cholesterol (E), and ROS (F) in control and MASLD model cells. (Data are expressed as mean \pm SD, * p < .05, ** p < .01, *** p < .001 compared with the controls using two-tailed Student's t-test, n = 3).

RNA (miscRNA), small nuclear RNA (snRNA), ribosomal RNA (rRNA), small nucleolar RNA (snoRNA), and microRNA (miRNA), and most of them are distributed on mRNA and lncRNA (Fig. 3A). Besides, among ac4C-modified transcripts, a significant number of RNA acetylation sites spanning 2 or more exons were identified (40% in the control group, 38.6% in the model group) (Fig. 3B). According to the results of the single base site analysis, the majority of ac4C-modified transcripts were found to have one ac4C modification site in both of two groups (28% for control group, 28.5% for model group). Intriguingly, another large proportion of the ac4C-

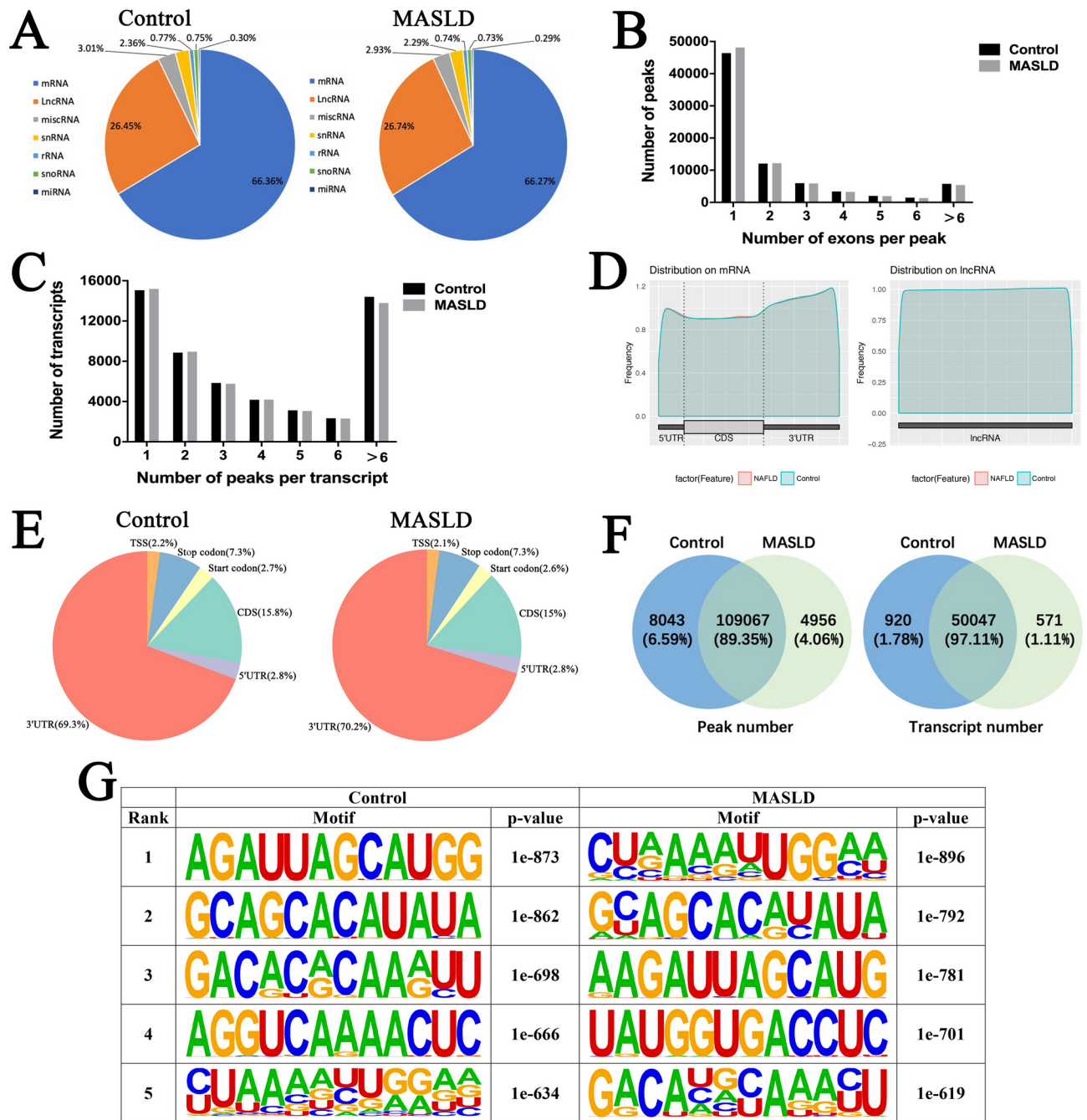


Fig. 3. Overview of ac4C peaks in control and MASLD model cells. **(A)** Distribution of ac4C sites on transcriptome in control and MASLD model cells. **(B)** The number of ac4C peaks spanning different number of exons in control and MASLD model cells. **(C)** The number of transcripts containing different number of ac4C peaks in control and MASLD model cells. **(D)** Distribution of ac4C peaks occurring within CDS or UTRs in mRNA and lncRNA regions in control and MASLD model cells. **(E)** The distribution of ac4Cs on mRNA in control and MASLD model cells within the 5' UTR, CDS, start codon, stop codon, TSS, and 3' UTR. **(F)** The overlaps and differences of ac4C peaks and ac4C modified transcripts between control and MASLD model cells. **(G)** The sequence logo of the top 5 differential mode motifs of ac4Cs from control and MASLD model cells.

modified transcripts were found to have more than six ac4C modification sites (26.7% for control group, 25.8% for model group) (Fig. 3C).

The acetylome analysis showed that most of ac4C sites were located in 3'UTR (69.3% for control group, 70.2% for model group) and CDS (15.8% for control group, 15% for model group) on mRNAs (Fig. 3D–E). Besides, ac4C modification showed no distribution specificity on lncRNAs (Fig. 3D right panel). The results of the intersection analysis between control and MASLD model groups revealed that 109,067 ac4C peaks were overlapped between the two groups, whereas 50,047 ac4C modified transcripts were overlapped. In addition, 4956 unique ac4C peaks correspond to 571 unique ac4C modified transcripts were observed in MASLD model cells (Fig. 3F). Homer de novo motif analysis results showed that the top five ac4C peak motifs in both groups comprised the typical ac4C motif “CXX” (Fig. 3G).

Distribution and functional pathways of differentially acetylated ac4C sites in control and MASLD model cells

Among all ac4C peaks found in two groups, a total of 2128 differentially acetylated ac4C sites were identified (fold change > 2; FDR < 0.05), of which 1031 hyperacetylated and 1097 hypoacetylated peaks were detected in MASLD model cells comparing with those in control cells (Fig. 4A). The number of up- and down-regulated acetylated ac4C sites on chromosomes is shown in Fig. 4B, with the top ten hyper- and hypoacetylated peaks listed in Table 2. Cluster analysis revealed a clear distinction in the ac4C acetylation patterns between control and MASLD model cells (Fig. 4C).

GO enrichment analysis was applied to reveal the potential functions of ac4C differentially modified genes (ADMGs) in MASLD model cells. In biological processes (BP), we found that ADMGs were significantly enriched in 710 GOs, including nuclear transport, nucleocytoplasmic transport, and mRNA processing (Fig. 4D). In cellular components (CC), 158 GO terms were significantly enriched, including cell–substrate junction, cell–substrate adherens junction, and focal adhesion (Fig. 4E). In molecular functions (MF), 76 GO terms were enriched, such as cell adhesion molecule binding, cadherin binding, and actin binding (Fig. 4F). KEGG enrichment analysis was further utilized to analyze the pathways associated with ADMGs in MASLD model cells. For hyperacetylated ADMGs enrichment, 184 pathways were identified, of which 27 pathways were significantly enriched. For hypoacetylated ADMGs enrichment, there were 182 pathways discovered, with 30 pathways terms significantly enriched. Moreover, the hyperacetylated ADMGs were mostly enriched in MAPK signaling pathway, endocytosis, and focal adhesion (Fig. 4G), while the hypoacetylated ADMGs were mainly enriched in pathways in cancer, focal adhesion, and RNA transport (Fig. 4H).

Whole-transcriptome profiling of gene expression and functional enrichment of differentially expressed genes (DEGs) in control and MASLD model cells

To investigate the expression of phenotype-related genes, the DEGs between control and MASLD model groups were analyzed. Gene counts were standardized by fragments per kilo base million reads (FPKM). The box plot indicated that standardization was good with no significant bias among groups (Fig. 5A). As illustrated

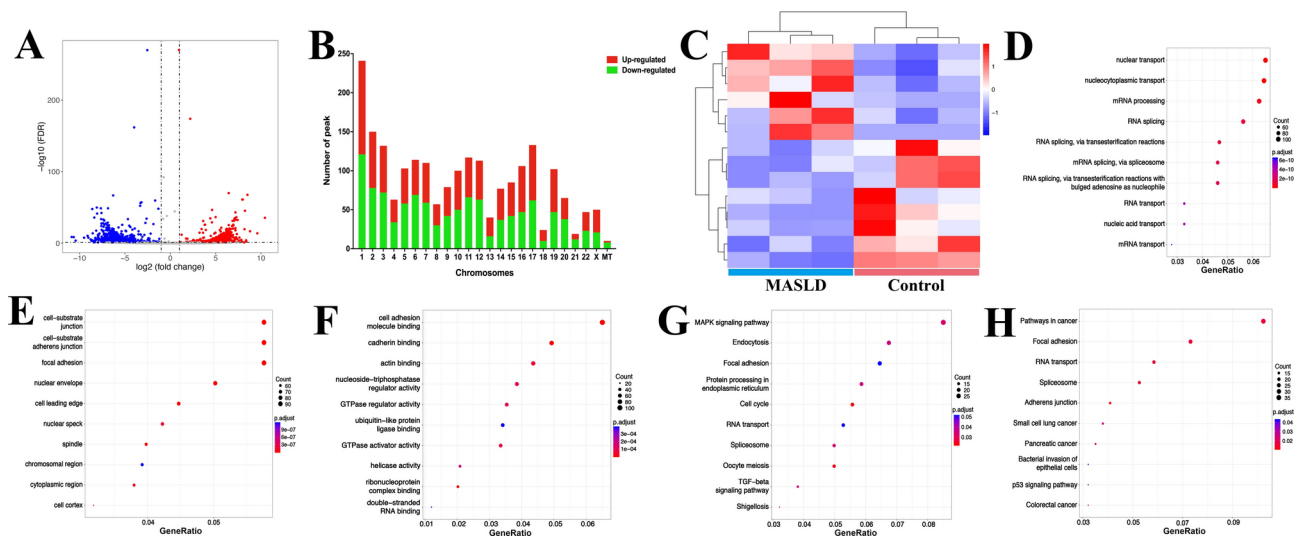


Fig. 4. Overview of the distribution of differentially acetylated ac4C sites in control and MASLD model cells. (A) Volcano plots of differential acetylated ac4C sites with statistical significance (fold change > 2; FDR < 0.05). Blue points indicate significantly down-regulated transcripts and red points indicate significantly up-regulated transcripts. (B) The distribution of differential ac4C peaks on chromosomes in control and MASLD model cells. (C) Heatmap of different ac4C modification patterns between control and MASLD model cells. GO enrichment map of ADMGs in (D) biological processes (BP), (E) cellular components (CC), (F) molecular functions (MF) categories. KEGG enrichment map of hyperacetylated (G) and hypoacetylated (H) ADMGs between control and MASLD model cells.

Ensembl gene ID	chromosome	thickStart	thickEnd	Gene name	Gene biotype	Acetylation status	Fold change
ENSG00000123560	X	103773717	103792619	PLP1	protein_coding	hyperacetylated	1448
ENSG00000163466	2	218253995	218254176	ARPC2	protein_coding	hyperacetylated	776
ENSG00000170265	7	149225259	149225440	ZNF282	protein_coding	hyperacetylated	443
ENSG00000117632	1	25900864	25901454	STMN1	protein_coding	hyperacetylated	383
ENSG00000183691	17	56593698	56595590	NOG	protein_coding	hyperacetylated	340
ENSG00000118922	13	73687285	73687705	KLF12	protein_coding	hyperacetylated	338
ENSG00000166848	16	75648443	75648623	TERF2IP	protein_coding	hyperacetylated	302
ENSG00000095787	10	28619877	28620088	WAC	protein_coding	hyperacetylated	292
ENSG00000161960	17	7578616	7578826	EIF4A1	protein_coding	hyperacetylated	254
ENSG00000179431	11	35619687	35620010	FJX1	protein_coding	hyperacetylated	241
ENSG00000139329	12	91102628	91111831	LUM	protein_coding	hypoacetylated	1783
ENSG00000164187	5	36100419	36100599	LMBRD2	protein_coding	hypoacetylated	1552
ENSG00000136104	13	50,970,092	50,973,506	RNASEH2B	protein_coding	hypoacetylated	1351
ENSG00000177640	10	118099095	118210153	CASC2	antisense_RNA	hypoacetylated	695
ENSG00000162695	1	100980615	100980796	SLC30A7	protein_coding	hypoacetylated	549
ENSG00000268043	1	146969592	146971286	NBPF12	protein_coding	hypoacetylated	501
ENSG00000006451	7	39707527	39707767	RALA	protein_coding	hypoacetylated	437
ENSG00000253967	8	70471133	70485687	LINC03020	lincRNA	hypoacetylated	393
ENSG00000160789	1	156139249	156139430	LMNA	protein_coding	hypoacetylated	388
ENSG00000249709	19	12525908	12526238	ZNF564	protein_coding	hypoacetylated	377

Table 2. Top 10 hyperacetylated and hypoacetylated peaks in MASLD model cells.

in Fig. 5B, 61 differentially expressed lncRNAs and 280 differentially expressed mRNAs were identified (fold change > 2, $P < 0.05$), with 31 lncRNAs and 136 mRNAs up-regulated, and 30 lncRNAs and 144 mRNAs down-regulated in MASLD model cells (Fig. 5C). The top ten up- and down-regulated genes in MASLD model cells are listed in Table 3. The cluster plot showed a clear expression pattern difference between control and MASLD model cells (Fig. 5D).

GO analysis was applied for functional classification of DEGs. In BP, 159 GOs were significantly enriched, mainly included in long-chain fatty acid biosynthetic process, macromolecule depalmitoylation, and collagen catabolic process (Fig. 5E). In CC, 18 GOs were significantly enriched, including collagen trimer, fibrillar collagen trimer, and banded collagen fibril (Fig. 5F). In MF, 33 GOs were significantly enriched, mainly involving palmitoyl–(protein) hydrolase activity, palmitoyl hydrolase activity, and integrin binding (Fig. 5G). KEGG pathway analysis linked up-regulated DEGs to beta-Alanine metabolism (Fig. 5H), and down-regulated DEGs to ECM–receptor interaction, systemic lupus erythematosus, and protein digestion and absorption (Fig. 5I).

Association analysis of differential ac4C modifications with differential gene expression in control and MASLD model cells

To explore the association of ac4C modification with gene expression, we cross-analyzed the acRIP-ac4c-seq and RNA-seq data. There are 4 types of association analysis results: Hyperacetylated-up (hyperacetylated ac4C modification and up-regulated RNA expression); hyperacetylated-down (hyperacetylated ac4C modification and down-regulated RNA expression); hypoacetylated-up (hypoacetylated ac4C modification and up-regulated RNA expression); hypoacetylated-down (hypoacetylated ac4C modification and down-regulated RNA expression). As illustrated in Fig. 6A a total of 118 genes were found both significantly changed in ac4C modification and expression levels in MASLD model cells (P value < 0.05). The PPI network analysis by cytoscape software showed that JUN, CAV1, FASN, and hnRNPA1 were core proteins among these 118 genes (Fig. 6B)¹⁴. Furthermore, consistent with the sequencing data, the mRNA and protein expression levels of CAV1 were significantly increased, whereas those of JUN, FASN, and hnRNPA1 were significantly decreased in MASLD model cells (Fig. 6C, D). These genes were reported to be involved in the lipid synthesis and metabolism^{15,16}. Moreover, the top 14 genes (red points in Fig. 6A), which were significantly changed in ac4C modification and expression levels with the highest fold change in MASLD model cells, are listed in Table 4.

Discussion

It is estimated that approximately 1.7 billion people globally suffer from MASLD, with an overall prevalence of approximately 25%⁴. Although the current research on MASLD has been in-depth and comprehensive, the exact pathogenesis of MASLD remains unclear due to its complex etiology.

FFAs, key lipotoxic factors, can cause insulin resistance, disorders of glucose-lipid metabolism and lipid peroxidation, and contribute to fatty liver induction^{17,18}. Esterification of excess FFA to triglyceride in hepatocytes leads to lipid accumulation in liver, resulting in hepatic steatosis¹⁹. In our study, a large accumulation of intracellular lipid droplets in HepaRG cells suggested that FFA successfully induced steatosis, which can be further used in the investigation of the pathogenesis of MASLD.

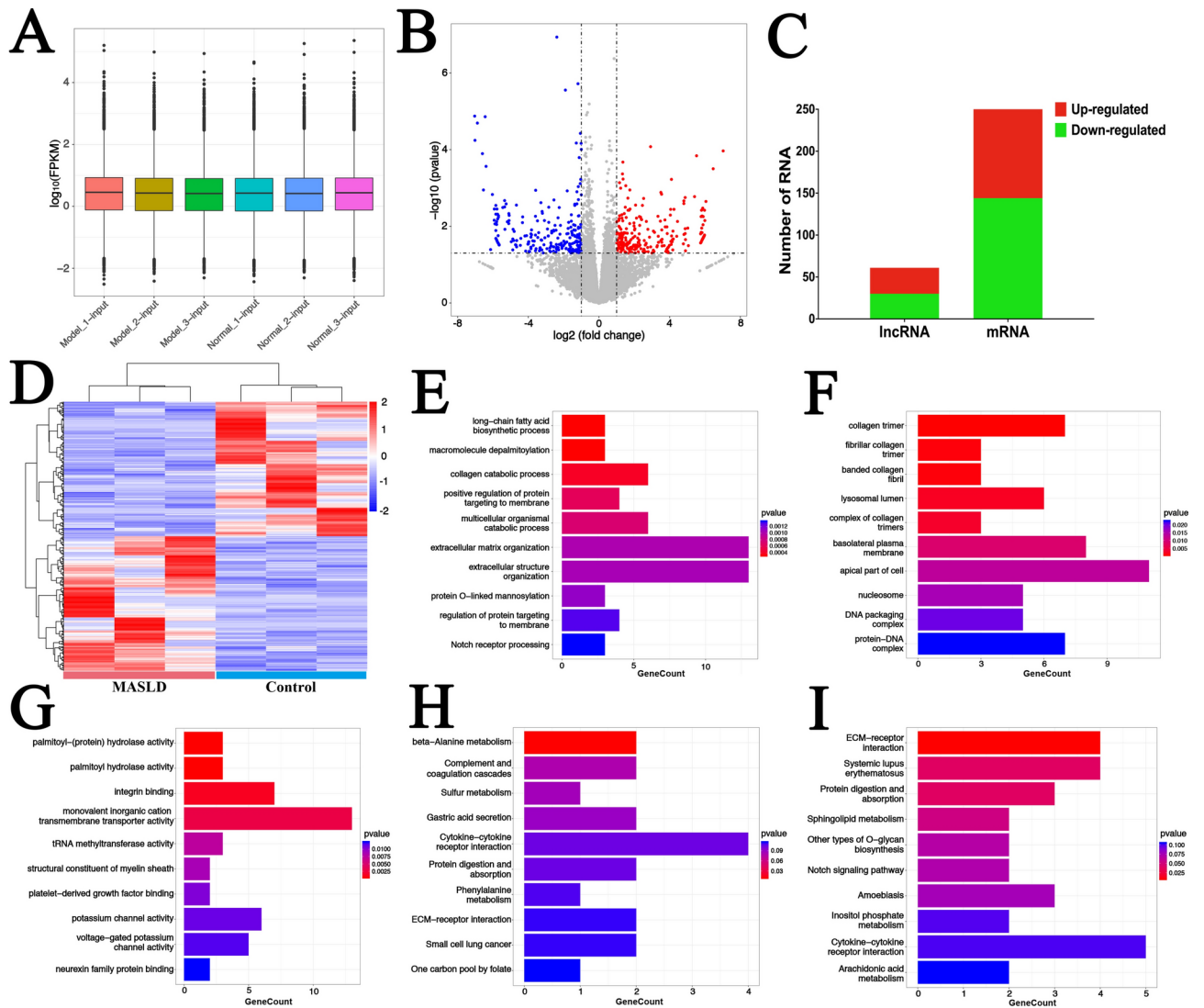


Fig. 5. Overview of gene expression and differentially expressed genes (DEGs) in control and MASLD model cells. **(A)** The distribution of gene expression in each cell sample after FPKM standardization. **(B)** Volcano plots of DEGs with statistical significance (fold change > 2; Pvalue < 0.05). Blue points indicate significantly down-regulated genes and red points indicate significantly up-regulated genes. **(C)** The distribution of differentially expressed lncRNAs and mRNAs in MASLD model cells. **(D)** Heatmap of DEGs patterns between control and MASLD model cells. GO enrichment map of DEGs in **(E)** biological processes (BP), **(F)** cellular components (CC), **(G)** molecular functions (MF) categories. KEGG enrichment map of up-regulated **(H)** and down-regulated **(I)** DEGs between control and MASLD model cells.

ac4C, similar to N6-methyladenosine (m6A), is a conserved RNA modification among eukaryotes. Previous studies have indicated that ac4C is primarily present on tRNA and 18S rRNA²⁰, but recent research has revealed its presence on mRNAs, where it plays a crucial role in promoting RNA stability and protein translation, positioning it as a promising area in epitranscriptomics^{8,21}. Advances in understanding ac4C have demonstrated its involvement in the progression of various human diseases²². Much of the current research has focused on the role of ac4C in cancers, such as colon, bladder, breast, and gastric cancers^{23–26}. Other studies have evidenced that ac4C modification also influences autoimmune, chronic, and infectious diseases. Guo et al. found that ac4C modification and the expression of acetyltransferase NAT10 was decreased in CD4⁺ T cells of SLE patients. Meanwhile, functional enrichments indicated that ac4C modification was involved in biological process of SLE progression¹¹. Another study documented that NAT10 increased the replication of HIV-1 by adding ac4C to HIV-1 RNA, thus facilitating HIV-1 disease progression¹². Dodson et al. reported that ac4C levels on murine tRNA^{lnc(CAU)} were increased in heart tissues from type II diabetic mice model, indicating that ac4C modification was associated with diabetes²⁷. Additionally, the studies on RNA chemical modifications in disease has demonstrated that ac4C is involved in sepsis, myocardial infarction, and Alzheimer's disease^{28–30}. However, whether ac4C modification plays a role in MASLD remains unclear. In this study, using an in vitro MASLD model induced by FFA, we identified that ac4C modification plays a vital role in biological processes of MASLD

LncRNA				mRNA			
Ensembl gene ID	Gene name	Expression status	Fold change	Ensembl gene ID	Gene name	Expression status	Fold change
ENSG00000262898	AC139099.2	up	66	ENSG00000117586	TNFSF4	up	88
ENSG00000273568	AC131009.3	up	63	ENSG00000149968	MMP3	up	64
ENSG00000249584	LINC02225	up	59	ENSG00000087495	PHACTR3	up	62
ENSG00000259457	AC100826.1	up	55	ENSG00000149452	SLC22A8	up	61
ENSG00000278991	AC090181.3	up	43	ENSG00000122176	FMOD	up	60
ENSG00000260949	AP006545.1	up	28	ENSG00000137726	FXYP6	up	60
ENSG00000235314	LINC00957	up	19	ENSG00000203942	C10orf62	up	60
ENSG00000266538	AC005838.2	up	18	ENSG00000198719	DLL1	up	58
ENSG00000253633	AP002852.2	up	17	ENSG00000131668	BARX1	up	58
ENSG00000224318	CHL1-AS2	up	16	ENSG00000181634	TNFSF15	up	57
ENSG00000280311	AC131212.4	down	57	ENSG00000204262	COL5A2	down	130
ENSG00000251161	AC020661.1	down	52	ENSG00000168542	COL3A1	down	118
ENSG00000214548	MEG3	down	50	ENSG00000177076	ACER2	down	71
ENSG00000273162	AL133215.2	down	43	ENSG00000128482	RNF112	down	57
ENSG00000261167	AC107027.3	down	34	ENSG00000072182	ASIC4	down	57
ENSG00000242767	ZBTB20-AS4	down	29	ENSG00000117400	MPL	down	57
ENSG00000270673	YTHDF3-AS1	down	28	ENSG00000165125	TRPV6	down	57
ENSG00000224167	AL390729.1	down	26	ENSG00000143845	ETNK2	down	56
ENSG00000170161	AL512625.1	down	18	ENSG00000170381	SEMA3E	down	56
ENSG00000279873	LINC01126	down	16	ENSG00000116254	CHD5	down	56

Table 3. Top 10 up-regulated and down-regulated genes in MASLD model cells.

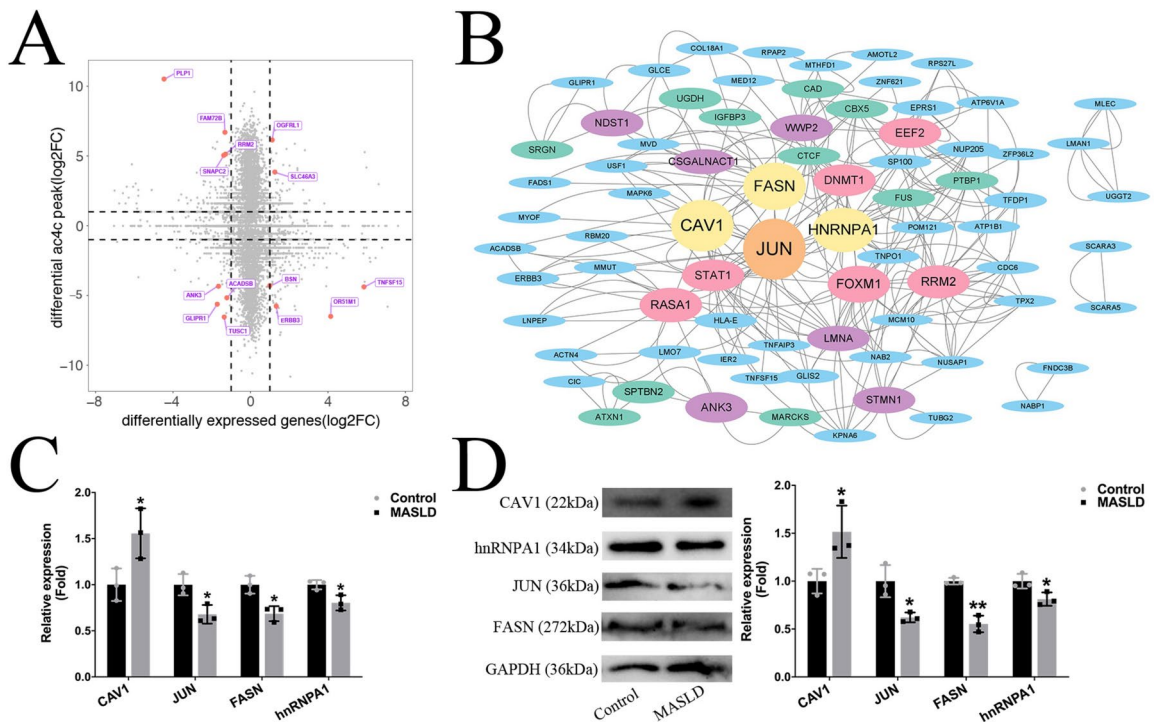


Fig. 6. Correlation of differential ac4C peaks with DEGs in control and MASLD model cells. **(A)** Scatter plot of genes with significant changes in ac4C modifications and RNA expression. **(B)** PPI network of genes with significant changes in ac4C modifications and RNA expression. **(C)** mRNA expression of JUN, CAV1, FASN, and HNRNPA1 in control and MASLD model cells. **(D)** Protein expression of JUN, CAV1, FASN, and HNRNPA1 in control and MASLD model cells. The full-length membranes were cropped prior to hybridisation with antibodies. The original images of all blots are presented in Supplementary information file. (Data are expressed as mean \pm SD, * $p < .05$, ** $p < .01$, *** $p < .001$ compared with the controls using two-tailed Student's t-test, $n = 3$).

Ensembl gene ID	Chromosome	thickStart	thickEnd	Gene name	Gene biotype	Acetylation and expression status
ENSG00000119900	6	71301967	71302148	OGFRL1	protein_coding	Hyperacetylated-up
ENSG00000139508	13	28700243	28700424	SLC46A3	protein_coding	Hyperacetylated-up
ENSG00000104976	19	7922414	7922594	SNAPC2	protein_coding	Hyperacetylated-down
ENSG00000123560	X	103773717	103792619	PLP1	protein_coding	Hyperacetylated-down
ENSG00000171848	2	10127105	10127255	RRM2	protein_coding	Hyperacetylated-down
ENSG00000188610	1	121181322	121183938	FAM72B	protein_coding	Hyperacetylated-down
ENSG00000065361	12	56095416	56095794	ERBB3	protein_coding	Hypoacetylated-up
ENSG00000151150	10	60026297	60029777	ANK3	protein_coding	Hypoacetylated-up
ENSG00000181634	9	114784634	114806126	TNFSF15	protein_coding	Hypoacetylated-up
ENSG00000184698	11	5390151	5393263	OR51M1	protein_coding	Hypoacetylated-up
ENSG00000139278	12	75499790	75500090	GLIPR1	protein_coding	Hypoacetylated-down
ENSG00000164061	3	49667825	49670975	BSN	protein_coding	Hypoacetylated-down
ENSG00000196177	10	123057263	123058311	ACADSB	protein_coding	Hypoacetylated-down
ENSG00000198680	9	25677220	25677400	TUSC1	protein_coding	Hypoacetylated-down

Table 4. Top 14 genes with significant changes in ac4C modification and expression levels in MASLD model cells.

progression. ac4Cs were mainly distributed in 3'UTR and CDS of transcripts in both control and MASLD model cells, which indicates that ac4C is a highly conserved and hardwired epitranscriptomic modification. Although we detected the aberrant ac4C modification in MASLD model cells, RNA-seq analysis revealed no significant differences in NAT10 expression between control and MASLD model cells, suggesting the potential involvement of other “writer(s)” in ac4C regulation in MASLD. Notably, we also identified 8 and 5 ac4C peaks on mitochondrial DNA (mtDNA) of control and MASLD model cells, respectively. Research has confirmed that mitochondrial dysfunction and dynamics are closely related to neurodegenerative and metabolic diseases, including MASLD³¹. Mposhi et al. reported that the methylation levels of mitochondrial NADH dehydrogenase subunit 6 (ND6) gene were increased in mice fed a high-fat diet (HFD) and in MASLD patients, and the induction of mtDNA methylation promoted mitochondrial dysfunction and interfered the lipid metabolism in liver cells^{32,33}. Therefore, whether the changes in ac4C level on the mtDNA can initiate MASLD progression by affecting mitochondrial function in liver remains to be determined.

To elucidate the potential functions of ADMGs and DEGs in MASLD model cells, we performed the GO and KEGG analysis for functional enrichment classification of these genes. GO analysis can be divided into three major groups: BP, CC, and MF. BP, being closest to phenotype, often reflects the biological state of the samples; CC describes gene localization within cells, which is significant for subcellular localization studies; MF explains the functional role of proteins, which is valuable when focusing on protein action changes within biological events³⁴. KEGG analysis has a more complete pathway annotation^{35,36}. The genes identified via the KEGG analysis are related to signaling pathways³⁷. Therefore, the purpose of KEGG analysis in this study was to find the signaling pathways that are significantly enriched in ac4c-modified gene. Here, KEGG analysis of hyperacetylated ADMGs indicated that MAPK signaling pathway was the most significantly enriched pathway. MAPK activation has been previously linked to exacerbation of hepatic steatosis and mitochondrial dysfunction, making it a notable molecular feature in MASLD progression^{38,39}. In addition, GO analysis of DEGs showed that long-chain fatty acid biosynthetic process was the most significantly enriched, including genes such as very long chain fatty acid-like family member 6 (ELOVL6), proteolipid protein 1 (PLP1), arachidonate 12-lipoxygenase, and 12R type (ALOX12B). ELOVL6 was proved to be positively correlated with MASLD progression and MASH pathology⁴⁰. The role of PLP1 and ALOX12B in MASLD progression remains unknown. Based on our GO and KEGG results for ADMGs and DEGs, we hypothesize that ac4C modification may regulate the stability and translation of lipid synthesis and metabolism-related genes, resulting in lipid homeostasis imbalance. This hypothesis requires further experimental validation.

The results of the association analysis of ac4C modification with gene expression showed that majority of the ac4C differential peaks has rather no effect on transcript abundance, which reminds us whether ac4C modification has a role in translational level of genes during MASLD progression. Since the regulation of gene expression is complex, in addition to ac4C modification, there may be other chemical modifications (such as m6A) or pathway regulation that may affect the transcription level of genes. Therefore, the exact role of ac4C modification in the MASLD progression requires further in-depth studies.

We further applied cytoscape software to investigate the interaction relationships among the genes both significantly changed in ac4C modification and expression levels in MASLD model cells. JUN, CAV1, FASN, and hnRNPA1 were identified as the core genes after network analysis by cytoscape. JUN, also known as c-Jun and AP-1, can regulate the transcription of many genes through binding to their promoters. Xie et al. has proved that the activation of JUN promoted hepatic steatosis by upregulating lipogenic gene expression⁴¹. CAV1, a structural and signaling protein of caveolae on cytoplasmic membrane, was evidenced to be positively associated with development of MASLD^{42,43}. FASN, a key enzyme driving the de novo lipogenesis (DNL) in the liver, was found to be increased in liver of MASLD patients and obese diabetic mice with MASLD^{44,45}. Epitranscriptome analysis has reported that increased FASN expression and m6A modification in MASLD model mice, underscoring its

central role in MASLD progression⁴⁶. Additionally, Wang et al. has found that long noncoding RNA suppressor of hepatic gluconeogenesis and lipogenesis (lncSHGL) repressed hepatic lipogenesis in HFD mice by recruiting hnRNPA1¹⁶. Therefore, the signaling pathways related to these four core genes are strongly implicated in molecular and PPI network associated with MASLD. However, inconsistent with previous findings, our study observed decreased expression of JUN, FASN, and hnRNPA1, with only CAV1 elevated in MASLD model cells. Therefore, further mechanistic studies on these proteins and MASLD progression are warranted.

Conclusions

The present study elucidates a transcriptome-wide ac4C modified profile of MASLD model cells. The altered expression of genes related to lipid synthesis and metabolism pathways, regulated by aberrant ac4C RNA acetylation, suggests a notable association between ac4C modification and MASLD progression. Collectively, our findings offer new insights into MASLD pathogenesis, and indicating the therapeutic potential of targeting ac4C-modified genes in prevention and management of MASLD.

Data availability

The datasets generated during the current study are available in NCBI SRA accession PRJNA1168032.

Received: 18 September 2024; Accepted: 24 December 2024

Published online: 06 January 2025

References

- Zhou, J. et al. Epidemiological features of NAFLD From 1999 to 2018 in China. *Hepatology* **71**, 1851–1864 (2020).
- Masoodi, M. et al. Metabolomics and lipidomics in NAFLD: Biomarkers and non-invasive diagnostic tests. *Nat. Rev. Gastroenterol. Hepatol.* **18**, 835–856 (2021).
- Loomba, R., Friedman, S. L. & Shulman, G. I. Mechanisms and disease consequences of nonalcoholic fatty liver disease. *Cell* **184**, 2537–2564 (2021).
- Powell, E. E., Wong, V. W. & Rinella, M. Non-alcoholic fatty liver disease. *Lancet* **397**, 2212–2224 (2021).
- Wiener, D. & Schwartz, S. The epitranscriptome beyond m(6)A. *Nat Rev Genet* **22**, 119–131 (2021).
- Dominissini D, Rechavi G. Epitranscriptome regulation. *Nat Struct Mol Biol* 2018.
- Zaccara, S., Ries, R. J. & Jaffrey, S. R. Reading, writing and erasing mRNA methylation. *Nat. Rev. Mol. Cell Bio.* **20**, 608–624 (2019).
- Arango, D. et al. Acetylation of cytidine in mRNA promotes translation efficiency. *Cell* **175**, 1872–86.e24 (2018).
- Sas-Chen, A. et al. Dynamic RNA acetylation revealed by quantitative cross-evolutionary mapping. *Nature* **583**, 638–643 (2020).
- Dominissini, D. & Rechavi, G. N(4)-acetylation of cytidine in mRNA by NAT10 regulates stability and translation. *Cell* **175**, 1725–1727 (2018).
- Guo, G. et al. Epitranscriptomic N4-acetylcytidine profiling in CD4(+) T cells of systemic lupus erythematosus. *Front Cell Dev Biol* **8**, 842 (2020).
- Tsai, K. et al. Acetylation of cytidine residues boosts HIV-1 gene expression by increasing viral RNA Stability. *Cell Host Microbe* **28**, 306–12.e6 (2020).
- Liu, Y., Xu, W., Zhai, T., You, J. & Chen, Y. Silibinin ameliorates hepatic lipid accumulation and oxidative stress in mice with non-alcoholic steatohepatitis by regulating CFLAR-JNK pathway. *Acta Pharm. Sin. B* **9**, 745–757 (2019).
- Shannon, P. et al. Cytoscape: A software environment for integrated models of biomolecular interaction networks. *Genome Res.* **13**, 2498–2504 (2003).
- Nassir, F. NAFLD: Mechanisms, treatments, and biomarkers. *Biomolecules* **12**, 824 (2022).
- Wang, J. et al. Long Noncoding RNA lncSHGL Recruits hnRNPA1 to Suppress Hepatic Gluconeogenesis and Lipogenesis. *Diabetes* **67**, 581–593 (2018).
- Boden, G. Interaction between free fatty acids and glucose metabolism. *Curr. Opin. Clin. Nutr.* **5**, 545–549 (2002).
- Delarue, J. & Magnan, C. Free fatty acids and insulin resistance. *Curr. Opin. Clin. Nutr.* **10**, 142–148 (2007).
- Zhang, J. et al. Association between serum free fatty acid levels and nonalcoholic fatty liver disease: A cross-sectional study. *Sci. Rep.-UK* **4**, 5832 (2014).
- Dong, C. et al. tRNA modification profiles of the fast-proliferating cancer cells. *Biochem. Biophys. Res. Commun.* **476**, 340–345 (2016).
- Castello, A. et al. Insights into RNA biology from an atlas of mammalian mRNA-binding proteins. *Cell* **149**, 1393–1406 (2012).
- Luo, J., Cao, J., Chen, C. & Xie, H. Emerging role of RNA acetylation modification ac4C in diseases: Current advances and future challenges. *Biochem. Pharmacol.* **213**, 115628 (2023).
- Deng, M. et al. Helicobacter pylori-induced NAT10 stabilizes MDM2 mRNA via RNA acetylation to facilitate gastric cancer progression. *J. Exp. Clin. Cancer Res.* **42**, 9 (2023).
- Wang, G. et al. NAT10-mediated mRNA N4-acetylcytidine modification promotes bladder cancer progression. *Clin. Transl. Med.* **12**, e738 (2022).
- Zheng, X. et al. N-acetyltransferase 10 promotes colon cancer progression by inhibiting ferroptosis through N4-acetylation and stabilization of ferroptosis suppressor protein 1 (FSP1) mRNA. *Cancer Commun.* **42**, 1347–1366 (2022).
- Zhang, X. et al. Revealing the potential markers of N(4)-Acetylcytidine through acRIP-seq in triple-negative breast cancer. *Genes* **13**, 2400 (2022).
- Dodson, T. A. et al. Ribonucleosides from tRNA in hyperglycemic mammalian cells and diabetic murine cardiac models. *Life Sci.* **318**, 121462 (2023).
- Zhang, H. et al. NAT10 regulates neutrophil pyroptosis in sepsis via acetylating ULK1 RNA and activating STING pathway. *Commun. Biol.* **5**, 916 (2022).
- Wang, K. et al. PIWI-interacting RNA HAAPIR regulates cardiomyocyte death after myocardial infarction by promoting NAT10-mediated ac(4) C acetylation of Tfec mRNA. *Adv. Sci.* **9**, e2106058 (2022).
- Ma, Y. et al. Comprehensive analysis of long non-coding RNAs N4-acetylcytidine in Alzheimer's disease mice model using high-throughput sequencing. *J. Alzheimers Dis.* **90**, 1659–1675 (2022).
- Peng, K. Y. et al. Mitochondrial dysfunction-related lipid changes occur in nonalcoholic fatty liver disease progression. *J. Lipid Res.* **59**, 1977–1986 (2018).
- Mposhi, A. et al. Mitochondrial DNA methylation in metabolic associated fatty liver disease. *Front. Nutr.* **10**, 964337 (2023).
- van der Wijst, M. G., van Tilburg, A. Y., Ruiters, M. H. & Rots, M. G. Experimental mitochondria-targeted DNA methylation identifies GpC methylation, not CpG methylation, as potential regulator of mitochondrial gene expression. *Sci. Rep.-UK* **7**, 177 (2017).
- Ashburner, M. et al. Gene ontology: tool for the unification of biology the gene ontology consortium. *Nat. Genet.* **25**, 25–29 (2000).

35. Kanehisa, M. & Goto, S. KEGG: kyoto encyclopedia of genes and genomes. *Nucleic Acids Res* **28**, 27–30 (2000).
36. Kanehisa, M., Sato, Y., Kawashima, M., Furumichi, M. & Tanabe, M. KEGG as a reference resource for gene and protein annotation. *Nucleic Acids Res.* **44**, D457–D462 (2016).
37. Draghici, S. et al. A systems biology approach for pathway level analysis. *Genome Re* **17**, 1537–1545 (2007).
38. Bai, L. et al. Multispecies transcriptomics identifies SIKE as a MAPK repressor that prevents NASH progression. *Sci. Transl. Med.* **16**, eade7347 (2024).
39. Ding, J. et al. HADHA alleviates hepatic steatosis and oxidative stress in NAFLD via inactivation of the MKK3/MAPK pathway. *Mol. Biol. Rep.* **50**, 961–970 (2023).
40. Matsuzaka, T. et al. Elovl6 promotes nonalcoholic steatohepatitis. *Hepatology* **56**, 2199–2208 (2012).
41. Xie, D. et al. High uric acid induces liver fat accumulation via ROS/JNK/AP-1 signaling. *Am. J. Physiol-Endoc. M* **320**, E1032–E1043 (2021).
42. Deng, G. H. et al. Caveolin-1 is critical for hepatic iron storage capacity in the development of nonalcoholic fatty liver disease. *Military Med. Res.* **10**, 53 (2023).
43. Xue, W. et al. Caveolin-1 alleviates lipid accumulation in NAFLD associated with promoting autophagy by inhibiting the Akt/mTOR pathway. *Eur. J. Pharmacol.* **871**, 172910 (2020).
44. Mitsuyoshi, H. et al. Analysis of hepatic genes involved in the metabolism of fatty acids and iron in nonalcoholic fatty liver disease. *Hepatol. Res.* **39**, 366–373 (2009).
45. Matsukawa, T. et al. Hepatic FASN deficiency differentially affects nonalcoholic fatty liver disease and diabetes in mouse obesity models. *JCI Insight* **8**, e161282 (2023).
46. Luo, Y. et al. Analysis of N6-methyladenosine methylation modification in fructose-induced non-alcoholic fatty liver disease. *Front. Endocrinol.* **12**, 780617 (2021).

Acknowledgements

We thank Prof. Ting Wang for her help in experiments and her constructive comments.

Author contributions

Xiqian Zhang designed and directed studies, analyzed and interpreted data, and drafted the manuscript. Yujie Yang and Fangyi Long suggested experiments, supervised the study, and revised the manuscript. Yaxian Zheng, Jing Yang, and Yan Yang performed cell experiments and data bioinformatics analysis. Qin He and Min Xu contributed to the discussion. All authors read and approved the final manuscript.

Funding

This study was financially supported by Technological Innovation Project of Chengdu Science and Technology Department (No. 2024-YF05-00157-SN), Seedling Engineering Project of Sichuan Science and Technology Department (No. 2022JDRC0145), Cultivation Project of Sichuan Science and Technology Department (Nos. 2022088, 2022089), and Chengdu Medical Research Project (No. 2024090).

Declarations

Competing interests

The authors declare no competing interests.

Additional information

Supplementary Information The online version contains supplementary material available at <https://doi.org/10.1038/s41598-024-84564-0>.

Correspondence and requests for materials should be addressed to F.L. or Y.Y.

Reprints and permissions information is available at www.nature.com/reprints.

Publisher's note Springer Nature remains neutral with regard to jurisdictional claims in published maps and institutional affiliations.

Open Access This article is licensed under a Creative Commons Attribution-NonCommercial-NoDerivatives 4.0 International License, which permits any non-commercial use, sharing, distribution and reproduction in any medium or format, as long as you give appropriate credit to the original author(s) and the source, provide a link to the Creative Commons licence, and indicate if you modified the licensed material. You do not have permission under this licence to share adapted material derived from this article or parts of it. The images or other third party material in this article are included in the article's Creative Commons licence, unless indicated otherwise in a credit line to the material. If material is not included in the article's Creative Commons licence and your intended use is not permitted by statutory regulation or exceeds the permitted use, you will need to obtain permission directly from the copyright holder. To view a copy of this licence, visit <http://creativecommons.org/licenses/by-nc-nd/4.0/>.

© The Author(s) 2025